NANO LETTERS

Letter

pubs.acs.org/NanoLett

Highly Controllable and Stable Quantized Conductance and Resistive Switching Mechanism in Single-Crystal TiO_2 Resistive Memory on Silicon

Chengqing Hu,[†,‡] Martin D. McDaniel,[§] Agham Posadas,[∥] Alexander A. Demkov,[∥] John G. Ekerdt,[§] and Edward T. Yu*[,†,‡]

[†]Microelectronics Research Center, [‡]Department of Electrical and Computer Engineering, [§]Department of Chemical Engineering, and [∥]Department of Physics, The University of Texas at Austin, Austin, Texas 78758, United States

Supporting Information

ABSTRACT: TiO_2 is being widely explored as an active resistive switching (RS) material for resistive random access memory. We report a detailed analysis of the RS characteristics of single-crystal anatase-TiO_2 thin films epitaxially grown on silicon by atomic layer deposition. We demonstrate that although the valence change mechanism is responsible for the observed RS, single-crystal anatase-TiO_2 thin films show electrical characteristics that are very different from the usual switching behaviors observed for polycrystalline or amorphous TiO_2 and instead very similar to those found in electrochemical metallization memory. In addition, we demonstrate highly stable and reproducible quantized conductance that is well controlled by application of a compliance current and that suggests the localized formation of conducting Magnéli-like nanophases. The quantized conductance observed results in multiple well-defined resistance states suitable for implementation of multilevel memory cells.

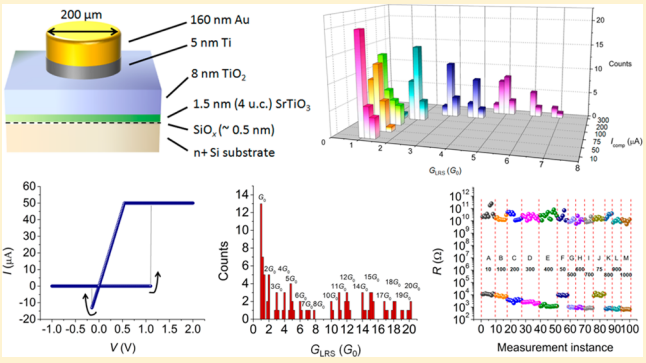

KEYWORDS: *Quantized conductance, nanofilament, multilevel resistive switching, valence change memory, titanium dioxide, single-crystal*

In recent years there has been intense interest in developing noncharge-based nanoscale nonvolatile memory (NVM) bit cells as an alternative to the current mainstream charge-based approaches as represented by flash memories, which suffer from long writing times and face tremendous challenges as transistor sizes decrease further into the nanoscale regime.[1] Among the emerging NVM technologies, metal-oxide resistive random access memory (RRAM) has received particular interest owing to its high density, excellent scalability, simple device structures, low power consumption, fast switching speed, and compatibility with conventional complementary metal-oxide-semiconductor (CMOS) technology.[2−4]

TiO_2 is one of the most extensively studied metal oxides that exhibit resistive switching (RS) behavior and has enjoyed particular prominence for RRAM applications, memristors, reconfigurable analog integrated circuits, stateful implication logic, and neuromorphic computing.[5−19] In addition, TiO_2 is particularly intriguing in that both unipolar RS (URS) and bipolar RS (BRS) have been reported,[15] enabling it to serve as a rich platform for studying and comparing different RS mechanisms concurrently,[3,5] including thermochemical,[12,13] valence change,[8] and electrostatic/electronic switching.[14,17] Regardless of the specific RS behavior that TiO_2 demonstrates, oxygen vacancies are always believed to play a critical role in the RS of TiO_2, as indicated both theoretically[20,21] and experimentally.[6,7,19,22,23] In this work, RS of single-crystal anatase TiO_2 grown epitaxially on Si(001) is investigated in detail and shown to originate from a valence change mechanism rather than thermochemical or electrostatic/electronic switching but to behave electrically in a manner very similar to electrochemical metallization memory and quite different from typical polycrystalline or amorphous TiO_2 RS elements.[5−9,12−19,22,23] Key characteristics of the RS we observe in single-crystal anatase TiO_2 include a high ON/OFF ratio (10^6−10^7), small electronic leakage current in the high-resistance state (HRS),[24] low RESET current, and highly controllable and reproducible quantized conductance (QC) in the low-resistance state (LRS).

For many RRAMs, the formation and rupture of nanoscale conductive filaments (CF) within an insulating matrix is widely accepted as the major working mechanism.[2,3] In fact, the prediction that ideally a CF can be shrunk to the atomic scale has helped to trigger extensive research efforts in the RRAM field. Quantized conductance[25] for the low-resistance state of

Received: April 3, 2014
Revised: July 16, 2014
Published: July 29, 2014

   dx.doi.org/10.1021/nl501249q | *Nano Lett.* 2014, 14, 4360−4367

RS is an inevitable consequence of scaling of filamentary-type RRAM cells to nanoscale dimensions and has been suggested to be of potential interest for building synaptic devices.[26−28] For these reasons, combined with their compatibility with silicon-based CMOS technology, binary oxides have been a subject of intense research interest in recent years for demonstration and investigation of quantized conductance phenomena. Previous reports have shown that conductance quantization can occur in metal oxides or silicon oxide without using Ag or Cu as an active electrode.[29−34] However, these results are either associated with transient current jumps (i.e., conductance changes) during the SET/RESET process that significantly limit the usefulness of the observed QC or obtained from dc resistance recorded at a specific voltage in a nonlinear LRS current−voltage ($I-V$) characteristic, leading to ambiguity when interpreting the measured resistance. More importantly, effective control over stabilized QC of a nanofilament by electrical means is generally absent. Here, highly stable QC is unambiguously demonstrated in epitaxial single-crystal anatase TiO_2 RRAM cells with the number of quantized channels reproducibly controlled by the compliance current applied during the SET process. This behavior enables epitaxial TiO_2 RS devices to offer the possibility of working as a practical multilevel cell and as a platform for exploring novel electrical properties associated with metallic nanophases present in metal oxides.

Experimental Details. *Film Growth.* Epitaxial single-crystal anatase TiO_2 thin films of 8 nm thickness were grown by atomic layer deposition (ALD) on n+ Si(001) substrates ($\rho \sim 0.01$ Ω·cm) with a thin single-crystal strontium titanate (STO) buffer layer. The four unit cells of STO grown by molecular beam epitaxy (MBE) serve as a template for ALD growth. The TiO_2 film is crystalline as-deposited on STO-buffered Si(001) with no postdeposition annealing required. Additional details regarding growth and crystallinity of the TiO_2/STO/Si heterostructures can be found elsewhere.[35,36]

X-ray Photoelectron Spectroscopy. The TiO_2 films were analyzed by in situ X-ray photoelectron spectroscopy (XPS). For the 8 nm TiO_2 film, XPS spectra were taken before and after ALD growth. XPS is performed with a VG Scienta R3000 electron analyzer with a monochromated Al Kα X-ray source. The analyzer is calibrated using a silver foil, where the Ag $3d_{5/2}$ core level is defined to be 368.28 eV. High-resolution spectra of the Ti 2p, O 1s, and Si 2p peaks are measured using a pass energy of 100 eV with an analyzer slit width of 0.4 mm. Each high-resolution scan is measured four times and summed, using 50 meV steps with a dwell time 157 ms per step. Film composition was determined using CasaXPS (ver. 2.3.16) peak fitting with a Shirley background subtraction.

Device Fabrication and Characterization. Two hundred micrometer diameter circular top electrode contacts to the TiO_2 were formed by photolithography, e-beam evaporation of 5 nm Ti/160 nm Au, and lift-off. Metallic Ti overlayers deposited on TiO_2 (both bulk crystal and thin film) have been shown to produce a region of interfacial suboxide, TiO_x ($x < 2$). This interfacial layer is present even when Ti is deposited at a low temperature and is reported to be ∼2 nm thick.[37,38] Therefore, a nonstoichiometric TiO_x interlayer is expected at the top Ti/TiO_2 interface due to oxygen gettering by the metallic Ti overlayer.[8] The back surface of the n+ Si substrate was coated with 8 nm Ti/100 nm Au as a bottom electrode. The RS behavior of the films was measured in air at room temperature by an Agilent 4156A precision semiconductor parameter analyzer in $I-V$ sweep mode. The sweeping voltage V was applied to the top electrode with the bottom electrode grounded. The compliance current I_{comp} was fixed at 100 μA for electroforming, whereas during the SET process, I_{comp} was set between 10 μA and 1 mA to prevent hard breakdown in the TiO_2 films. The HRS and LRS resistances (R_{HRS} and R_{LRS}) were measured at a read voltage of +0.1 V.

Results and Discussion. Stoichiometric TiO_2 films were deposited on STO-buffered Si (001). High-resolution core-level spectra of the Si 2p, Ti 2p, Sr 3d, and O 1s were taken before and after TiO_2 film growth on the single-crystal STO buffer layer on Si (see Supporting Information). The Ti $2p_{3/2}$ peak is located at 459.4 eV for the 8 nm TiO_2 film, indicating that the Ti is fully oxidized. We note, however, that the sensitivity of XPS is not sufficient to detect oxygen deficiencies of much less than 1%, which can lead to significant changes in the electrical conductivity. While the presence of a low concentration of oxygen vacancies within the as-grown TiO_2 cannot, therefore, be excluded on the basis of XPS, electrical measurements indicate that the as-grown TiO_2 film is highly resistive. The Si 2p spectrum verifies that there is negligible SiO_2 formation after MBE growth of the single-crystal STO buffer layer. A small presence of silicon suboxide (SiO_x) is observed at ∼102.2 eV, although the thickness of this layer is estimated to be 5 Å or less.[35]

The device structure for the epitaxial TiO_2 RS cells is shown schematically in Figure 1a. The typical RS $I-V$ characteristics of

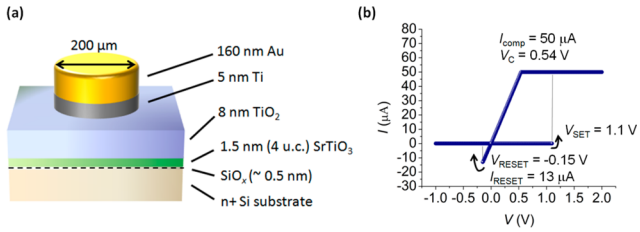

Figure 1. (a) Device structure for single-crystal TiO_2 cells; (b) typical $I-V$ characteristics.

such a device, shown in Figure 1b, exhibits linear $I-V$ behavior in the LRS and abrupt, clean RS for both SET and RESET processes. A detailed analysis of the electrical behavior provides important insights into the specific RS mechanism involved in this material system. There are five basic mechanisms that are used to explain redox-based RS in various materials:[3] the electrostatic/electronic mechanism, the valence change mechanism, the thermochemical mechanism,[39−41] the electrochemical metallization mechanism,[42] and the phase change mechanism.[43] For transition metal oxides such as TiO_2, the phase change mechanism, that is, temperature-induced transition between amorphous and crystalline phases, can be eliminated at the outset as the RS mechanism.[43] Detailed analysis of $I-V$ characteristics, as described below, allows all but one of the other mechanisms to be eliminated as well.

The electrostatic/electronic mechanism has been reported as a BRS mechanism in polycrystalline and amorphous TiO_2. In these materials, SET (RESET) occurs due to trapping (detrapping) of electrons in the switching layer (i.e., the layer adjacent to the top contact), which contains a high density of electron traps (typically oxygen vacancies), by applying a negative (positive) voltage to the top contact.[14,17] For the single crystal anatase TiO_2 films in our work, the oxygen-

dx.doi.org/10.1021/nl501249q | Nano Lett. 2014, 14, 4360−4367

deficient layer lies at the top of the structure, and therefore the bias voltage polarities for which the SET and RESET processes occur are contrary to those expected for the electrostatic/electronic mechanism. In addition, for RS devices that operate based on the electrostatic/electronic mechanism, space-charge-limited-current conduction governs electrical transport and leads to nonlinear (square-law) $I-V$ characteristics in the LRS, the ON/OFF ratio is usually small,[14,17] and there should be no sudden transition from the LRS to the HRS during RESET, all of which are contrary to the behavior found in this work. Thus, we conclude that the electrostatic/electronic-based mechanism is not responsible for the BRS of the single-crystal anatase TiO_2 films studied here.

RS via the thermochemical mechanism relies on rupture of CFs by self-accelerated diffusion of oxygen vacancies due to Joule heating and is responsible mainly for URS as well as BRS in some metal oxides.[39−41] In the case of thermochemical-based URS and BRS, the peak value of electric current during RESET, I_{reset}, is proportional to the compliance current, I_{comp}, with a universal ratio I_{reset}/I_{comp} of about 1.2, irrespective of the URS/BRS mode and of the metal oxide material used in the RRAM device.[39−41] For the TiO_2 devices in this work, however, I_{reset} is smaller than I_{comp} over a wide range of I_{comp}, as shown in Figure 2a, and the power dissipation at which RESET occurs is

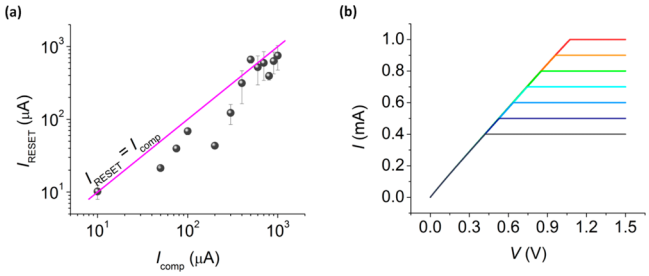

Figure 2. Electrical characteristics for the single-crystal TiO_2 device that contradict with those of thermochemical or heat-induced RS mechanism. (a) I_{RESET} versus I_{comp} for I_{comp} ranging from 10 μA to 1 mA; (b) $I-V$ characteristics of a set of dc double sweeps, each starting from V = 0 V but with an incremental I_{comp} (from 400 μA to 1 mA), after the SET process under I_{comp} = 400 μA.

therefore smaller than the power dissipated by the device in the ON state following the SET process for nearly all the different I_{comp} values tested. Figure 2b shows the $I-V$ characteristics of a set of dc double sweeps (i.e., an upsweep followed by a downsweep), each starting from V = 0 V but with I_{comp} increasing in 0.1 mA steps. The first sweep is with I_{comp} = 0.4 mA, right after the SET process under the same I_{comp}. It can be seen that for the following sweeps with I_{comp} incrementally increasing, R_{LRS} is always very stable and maintains the same value as that for the first sweep with I_{comp} = 0.4 mA. Even with I_{comp} for the last sweep at 1.0 mA, which is much larger than the corresponding $I_{reset} \sim$ 0.38 mA during the follow-up negative voltage sweep (not shown), R_{LRS} remains at the same value, indicating that the CF formed in the SET process is highly stable against either growing or rupturing. Positive voltage sweeps with I_{comp} = 10 mA and the same voltage peak value and sweep rate as for the former SET process (for which I_{comp} = 10 μA to 1 mA) were also performed (not shown); no URS behavior was observed under this condition. This observation together with Figure 2a,b unambiguously excludes the possibility of interpreting the RESET process as mainly being the result of heat-induced rupturing of the CF. It should be noted, however, that Joule heating could still play a minor role for the RESET processes in this material system, and thermochemical-based URS could potentially be achieved in our system by applying a voltage sweep with I_{comp} much larger than 10 mA.

The high ON/OFF ratio, low electronic leakage in the HRS, and linear $I-V$ characteristics in the LRS found for the single-crystal anatase TiO_2 devices are highly reminiscent of features typically observed in electrochemical-metallization based systems[3,26−28] in which a CF consisting of metal atoms with high ionic mobility (typically Ag or Cu) bridges the whole film during SET and mostly dissolves during RESET. However, in our material system Ti/Au is used as the top metal contact and titanium is not a highly mobile ionic species; in fact, positively charged oxygen vacancies are even more mobile than titanium ions[2,3] and are considered as the major mobile species driving the RS behavior in TiO_2.[3,6,7,20−23] Therefore, the only remaining possible mechanism that could be responsible for the RS observed in our material system is the valence change mechanism. Although this conclusion is consistent with previous reports on TiO_2 RRAM cells,[3,8] the electrical characteristics of single-crystal anatase TiO_2 RS devices are very different from, and generally superior to, those typically observed for amorphous or polycrystalline TiO_2.

Valence change-based BRS typically occurs in transition metal oxides with electrodes that do not inject metal cations because the electrode metal is not easily oxidized (e.g., Pt or Au) or that the oxidized form is not easily reduced back to the metal (e.g., Al, Ti, or Nb). This type of RS normally involves a localized (laterally for filamentary RS and vertically for interfacial area distributed RS) enrichment or depletion of oxygen vacancies by applying bias voltages of opposite polarities.[3] Interfacial RS based on the valence change mechanism relies on the modulation of a Schottky barrier by movement of an ionic species into or out of that barrier layer,[8] which typically shows electrode area-dependent R_{LRS}. In this respect, RS based on height and/or width modulation of a Schottky barrier is inconsistent with the linear LRS $I-V$ characteristics and abrupt transitions from the HRS to the LRS during RESET observed for our material system.[3,8] Figure 3a compares R_{LRS} (after SET at I_{comp} = 500 μA) for top electrodes of different sizes (80, 100, 150, and 200 μm in diameter, respectively), where R_{LRS} is found to be almost constant over different device sizes, suggesting the filamentary nature of the LRS. Shown in Figure 3b is R_{LRS} as a function of temperature

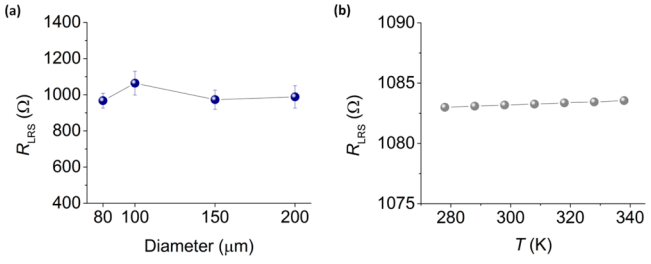

Figure 3. (a) R_{LRS} versus device size (in diameter) after SET processes (30 SET processes for each device size) under I_{comp} = 500 μA, showing no dependence of R_{LRS} on the device electrode area; (b) R_{LRS} versus T for a particular ON-state of the 200 μm diameter device after SET under I_{comp} = 500 μA, demonstrating a metallic conduction behavior in the LRS.

dx.doi.org/10.1021/nl501249q | Nano Lett. 2014, 14, 4360−4367

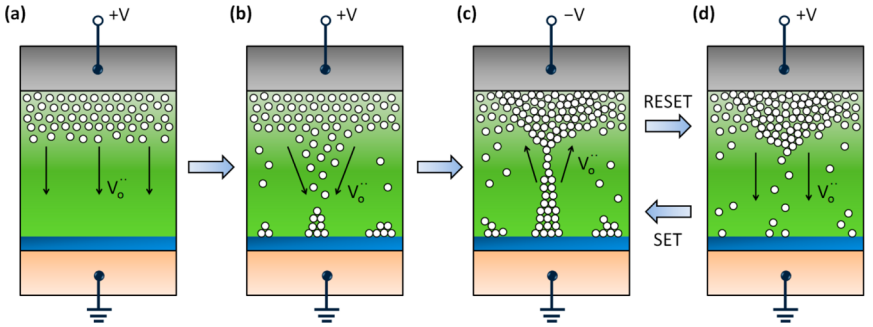

Figure 4. Illustration of the proposed RS mechanism based on the $I-V$ characteristics. In each part of the illustration, voltage is applied to the top contact after the depicted oxygen vacancy configuration is achieved within the TiO_2 matrix, and the arrows denote moving direction of oxygen vacancies upon application of voltage to the top contact. Oxygen vacancy configuration (a) in the pristine state, (b) during the SET process, (c) in the ON state, and (d) in the OFF state.

(278−338 K) around room temperature for a particular ON-state of the 200 μm device after SET at I_{comp} = 500 μA. R_{LRS} is clearly seen to be essentially constant, increasing by less than 1 Ω when the temperature increases from 278 to 338 K, indicating that ballistic conduction across a nanoscale channel with minimal additional series resistance, occurs. Therefore, we conclude that the filamentary-type valence change switching mechanism applies to the RS of our materials stack, that is, Au/Ti/single-crystal anatase TiO_2/STO/n+ Si.

The filamentary-type valence change based switching mechanism for the single-crystal TiO_2 device is therefore proposed to be as follows. In an as-fabricated TiO_2 device, an oxygen-deficient layer is only present at the top of the TiO_2 layer due to the top Ti metallization,[8] as shown in Figure 4a. We have determined experimentally that a single-crystal TiO_2 device is not switchable with a pure Au top electrode (specifically, for an 80 s double sweep of voltage with a peak voltage of +5 V). This behavior is different from that of conventional valence change memories in which oxygen vacancies can easily be generated at the interface with a noble-metal anode during electroforming and the resulting ON/OFF ratio is usually small.[3] This indicates that for a top electrode made of noble metal in contact with the single-crystal anatase TiO_2 film, the number of oxygen vacancies electrochemically generated during the electroforming/SET process (within the typical time scale employed in this work) is insufficient to form extended defects as the seed for a filamentary switching event.[3] In contrast, a top oxygen-deficient layer, serving as a reservoir of oxygen vacancies, helps to achieve a very high ON/OFF ratio without causing hard breakdown of the RS active layer.

By applying a positive bias voltage to the top contact, oxygen vacancies drifting from the top oxygen-deficient layer are partially reduced and redeposited upward from the bottom, that is, the TiO_2/STO interface (Figure 4b),[21] This process leads to localized formation of a CF, assisted by local roughness of the oxygen vacancy cluster distribution at the bottom that enables CF nucleation at a local asperity, to complete the SET process (Figure 4c). Since Ti_nO_{2n-1} (n = 3−5 for rutile and 5−7 for anatase) Magnéli or Magnéli-like nanophases are the only known structural configurations of oxygen vacancies in TiO_2 that demonstrate metallic and resistively switchable behaviors,[19,22,23,44] and the LRS $I-V$ behavior observed in this work is metallic (Figure 3b), we postulate that the CF formation in the anatase TiO_2 is attributable to an energetically favorable local phase transformation to a Magnéli-like nanophase by one-dimensional (laterally confined) nucleation of extended defects composed of migrating oxygen vacancies at a random site(s) for each SET process.[2,3,19,22] In addition, SET could also occur in the STO and/or SiO_x layers since the observed LRS $I-V$ characteristics is highly linear indicating the absence of a 2 nm thick STO/SiO_x tunnel barrier.

During the RESET process, the CF dissolves owing to the electrochemical current through the TiO_2 matrix, followed by the electric-field driven oxygen vacancy drift back to the top, as shown in Figure 4d. Figure 5a shows that the pristine-state current (i.e., OFF-state current before electroforming) is the same order of magnitude as the subsequent OFF-state current. This indicates that during the last stage of the RESET process [immediately after reaching the RESET voltage, −0.15 V in this

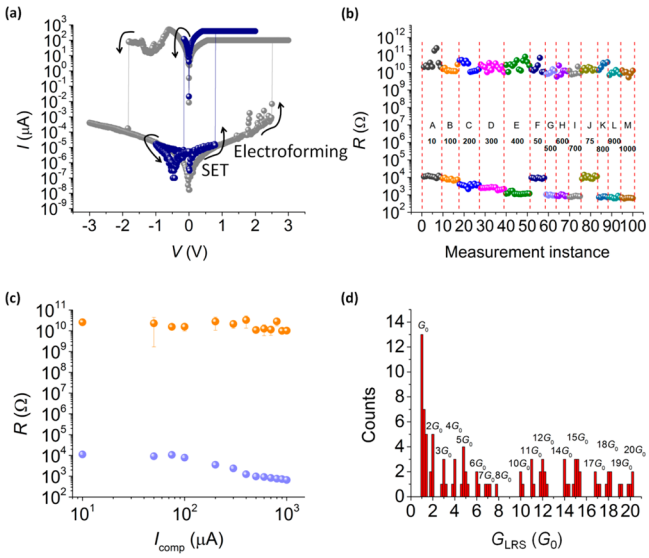

Figure 5. Electrical performance of an 8-nm-thick single-crystal TiO_2 device. (a) Log $I-V$ of typical RS characteristics of an electroforming sweep (gray) and a regular RS sweep (blue); (b) R_{HRS} and R_{LRS} over 100 successive switching sweeps with letters A−M indicating different I_{comp} applied during SET process of those sweeps (A, 10 μA; B, 100 μA; C, 200 μA; D, 300 μA; E, 400 μA; F, 50 μA; G, 500 μA; H, 600 μA; I, 700 μA; J, 75 μA; K, 800 μA; L, 900 μA; M, 1 mA); (c) R_{HRS} and R_{LRS} versus I_{comp} based on the data shown in (b), where saturation of the R_{LRS} increase at smaller I_{comp} can be seen; (d) histogram of G_{LRS} in units of $G_0 = 2e^2/h$ for the 100 successive cycles shown in (b) in which distribution of discrete peaks around integers of G_0 is clearly seen.

dx.doi.org/10.1021/nl501249q | Nano Lett. 2014, 14, 4360−4367

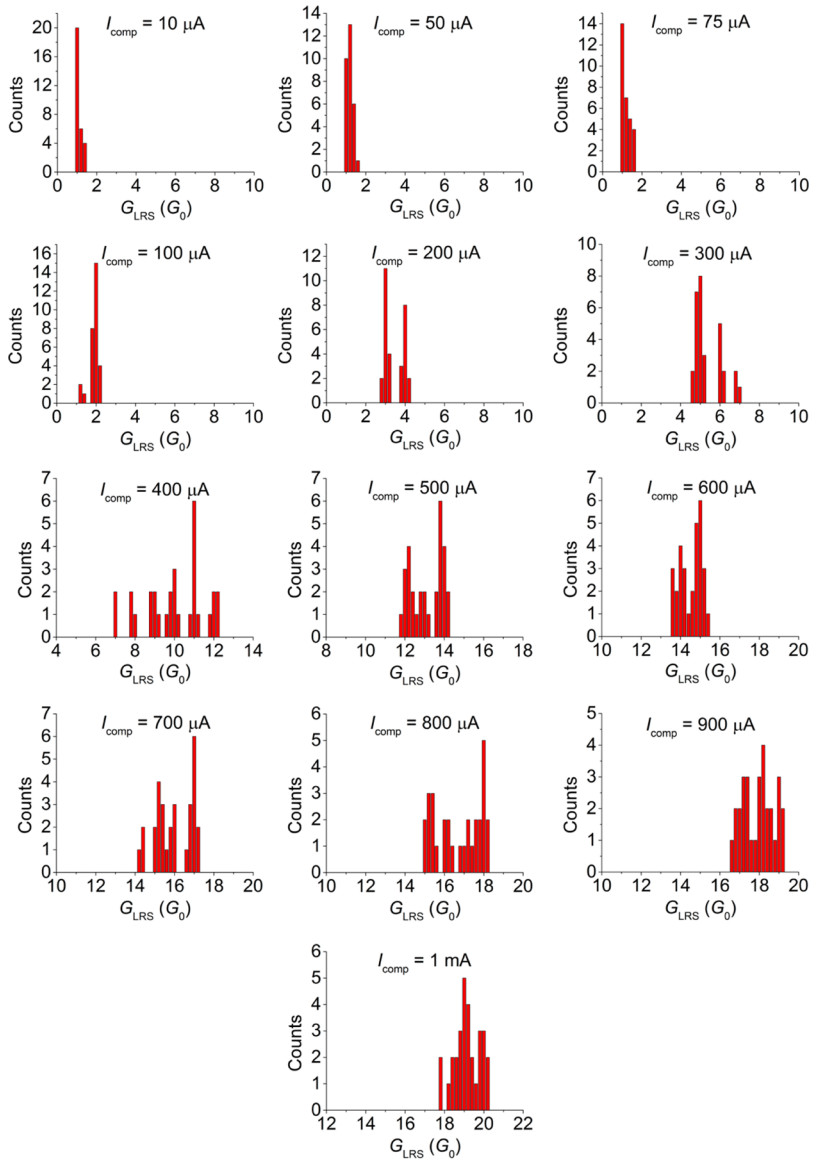

Figure 6. Histograms of G_{LRS} in units of $G_0 = 2e^2/h$ for the 390 cycles (including the 100 successive cycles in Figure 5) with 30 cycles for each I_{comp}, showing effective modulation of the number of quantized channels by varying I_{comp}.

case, cf. Figures 1b and 5a], most of the dissolved positively charged oxygen vacancies are driven by the large electric field back toward the top electrode, leaving the single-crystal anatase TiO_2 layer beneath with very few oxygen vacancies. On the other hand, the electroforming threshold voltage is higher than the SET voltage, as shown, for example, in Figure 5a and also observed for a wide range of SET compliance currents, indicating that during electroforming, additional oxygen vacancies are created by movement of oxygen atoms from the Ti/TiO_2 interface into the Ti electrode,[8] lowering the threshold voltage for the subsequent SET processes. We also note that in Figure 5a, the $I-V$ curve after RESET in the regular SET/RESET cycle does not go through the origin, which may indicate the emergence of the recently reported nanobattery effect for redox-based RS systems.[45]

Figure 5b shows R_{HRS} and R_{LRS} measured over 100 dc sweep cycles under I_{comp} ranging from 10 μA to 1 mA. Here, each R_{LRS} was measured right after a SET process under the corresponding I_{comp}, which is different from the measurement scenario for Figure 2b. Very high ON/OFF ratios of 10^6-10^7 are observed over the entire range of I_{comp}. This is unusual for filamentary-type valence change memory with a top electrode in the size range employed here (200 μm in diameter) for which the ON/OFF ratio is generally small because filamentary RS only affects a tiny portion of the entire electrode area and the remaining electrode area normally contributes to a nonswitching parallel resistance by means of electron tunneling or hopping through point defects (e.g., oxygen vacancies and/or reduced metal ions) within the insulating oxide matrix.[3] In this respect, the single-crystal nature of the TiO_2 could play a key role with high crystallinity and film quality helping to minimize the intrinsic defects and greatly suppress the background electric current in both states of RRAM operation. We also observe in Figure 5b that while no apparent trend of R_{HRS} over the cycles can be seen, a stable and reproducible modulation of R_{LRS} by over 1 order of magnitude is achieved by varying I_{comp}, indicating the potential of using the single-crystal anatase TiO_2 material system for implementation of multilevel memory cells.[3,4] Figure 5c shows R_{HRS} and R_{LRS} as a function of I_{comp} in the log R − log I form, summarizing the data from

dx.doi.org/10.1021/nl501249q | Nano Lett. 2014, 14, 4360−4367

Figure 5b. R_{HRS} is always above 10^{10} Ω over the entire range of I_{comp}, whereas R_{LRS} increases as I_{comp} decreases and eventually saturates at ∼12.9 kΩ. It should be noted that in our measurements, the SET process does not occur for I_{comp} < 10 μA from which we conclude that during the SET process a minimum compliance current is required to form and maintain a conductive nanofilament fully connecting the top and bottom electrodes. The saturation of R_{LRS} occurs at a resistance $R_0 = 1/G_0 = h/(2e^2)$, where h is Planck's constant and e is the magnitude of the electron charge. R_0 corresponds to the intrinsic contact resistance of a single-mode ballistic conductor sandwiched between two conductive contacts.[25]

The quantized nature of conductance in the LRS is shown more explicitly in Figure 5d in which a histogram of the LRS conductance $G_{LRS} \equiv 1/R_{LRS}$ for the 100 successive cycles shown in Figure 5b reveals a series of discrete peaks around integer multiples of G_0. To further elucidate the role of I_{comp} in determining the number of conductance channels n, histograms of G_{LRS} in units of G_0 for 390 switching cycles (30 cycles for each I_{comp}) performed on the same TiO_2 device as that for Figure 5 are shown in Figure 6 for compliance currents up to 1 mA. At compliance currents of 10−200 μA, histogram peak(s) corresponding to one or two quantized conductance values for each I_{comp} can be seen, and the number of conductance channels n increases with I_{comp}. Within this range of compliance current (10−200 μA), G_{LRS} can be controlled to within a single quantum of conductance by imposing a given I_{comp} during the device SET process. Since G_{LRS} is extracted from linear $I-V$ characteristics in the LRS, good control over n and therefore over the thickness of a conductive nanofilament at or near the atomic scale via I_{comp} is demonstrated. At all of the higher compliance currents tested (300 μA−1 mA), corresponding to larger numbers of conductance channels, n can be controlled to within $\pm(0.5-1.5)G_0$, with the average number of conductance channels increasing with I_{comp} and reaching $(19 \pm 0.6)G_0$ for I_{comp} = 1 mA. Figure 7a summarizes the data in Figure 6 by plotting G_{LRS} versus I_{comp} with the mean and standard deviation of G_{LRS} for each I_{comp} shown in Figure 7b. An almost linear dependence of G_{LRS} on I_{comp} can be observed, indicating that the voltage drop across the TiO_2 RRAM cell at the compliance current, labeled as V_C in Figure 1b, is roughly constant (∼0.5 V), consistent with the model of filament formation based on thermally activated and electric field driven oxygen vacancy migration.[39−41]

(a)

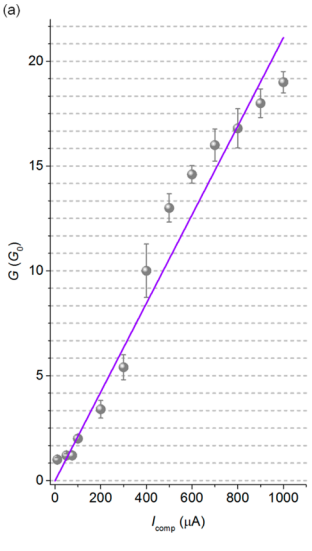

(b)

I_{comp} (μA)	Mean (G_0)	Std Dev (G_0)
10	1	0.1
50	1.2	0.1
75	1.2	0.2
100	2	0.2
200	3.4	0.5
300	5.4	0.7
400	10	1.5
500	13	0.8
600	14.6	0.5
700	16	0.9
800	16.8	1.1
900	18	0.8
1000	19	0.6

Figure 7. (a) G_{LRS} versus I_{comp} for I_{comp} ranging from 10 μA to 1 mA summarized from each histogram in Figure 6; (b) mean and standard deviation values of G_{LRS} in units of G_0 in (a).

The observation of highly controllable, reproducible QC raises the issue of the role the single-crystal anatase TiO_2 material system, including possible Magnéli-like nanophases, plays in demonstrating QC and whether the observed QC with multiple quantized channels, that is, for $n \geq 2$, corresponds to a single relatively thick nanofilament or a collection of independent thin nanofilaments.[46,47] With regard to the first issue, it has been previously reported that Magnéli-like nanocolumns of 1−2 nm in width can exist with (101) crystallographic shear planes in thin epitaxial anatase TiO_2 films grown on (001) $LaAlO_3$ planes,[44] and that SET switching can be regarded as a local phase transformation of the TiO_2 film (anatase or rutile) to the Magnéli or Magnéli-like phase at the nanometer scale.[2,3,19,22] It should be noted that R_{LRS} is essentially constant (with an increase by less than 1 Ω from 278 to 338 K) around room temperature for each ON-state (e.g., Figure 3b), also indicating that electron transport through the metallic CF is ballistic for which temperature-dependent scattering processes are generally absent. Therefore, the QC characteristics observed here in the LRS of the single-crystal anatase TiO_2 thin film are consistent with the localized formation of a filamentary quantized conductance channel consisting of a nanoscale Magnéli-like phase within which ballistic electron transport can occur. The bulk metal electrodes in contact with such a conductance channel could be either the Ti top and the n+ Si bottom electrodes, or thicker regions of metallic Magnéli-like phases that act as virtual metal electrodes connecting the atomic scale nanofilament to the Ti and n+ Si electrodes. In either case, the single-crystal nature and high quality of the anatase TiO_2 film is believed to play a key role in suppressing the background current and enabling the emergence of QC in the LRS.

With regard to the formation of a single filament or multiple filaments at high compliance currents, we see in Figure 2b that the CF is highly stable against further growth or rupturing at positive voltages once it is formed. In addition, it is widely known that regardless of the detailed RS mechanism, growth of a new CF is significantly suppressed after the cell is SET due to the combination of greatly decreased voltage drop across the cell upon SET and the exponential dependence of the CF growth rate on this voltage drop.[3,4] Therefore, if a collection of independent nanofilaments were to account for the higher values of G_{LRS}, they would need to form essentially simultaneously at the SET voltage. In this case, however, it is very unlikely that there would be such a clear monotonic dependence of n on I_{comp} (Figure 7), because the number of growing CFs before the cell is ON cannot be determined by I_{comp}. For $I_{comp} \geq 600$ μA, that is, $n \geq 14-16$, the observed distribution of values for G_{LRS} begins to become more continuous, as shown in Figure 6. This can be understood as a consequence of the fact that for a thicker conductive nanofilament, the energy spacing between its subbands becomes smaller and eventually is comparable to or smaller than a few k_BT, in which case sharp transitions of conductance over adjacent n's are significantly smeared out.[25] This also suggests the formation of a single thick nanofilament with a large n instead of a collection of several independent thin nanofilaments with small n's. It is therefore highly likely that

dx.doi.org/10.1021/nl501249q | Nano Lett. 2014, 14, 4360−4367

only a single thick nanofilament is formed for the cases where $n \geq 2$.

Conclusion. In this work, valence change-type BRS behavior observed in epitaxial single-crystal anatase TiO_2 thin film integrated on Si has been analyzed in detail, and highly controllable and reproducible quantized conductance has been demonstrated and analyzed. The electrical characteristics of the single-crystal anatase TiO_2 RRAM devices are shown to be very similar to those of electrochemical metallization rather than valence-change memory. Analysis of $I-V$ characteristics reveals the metallic filamentary nature of the LRS and that the filamentary-type valence-change effect is responsible for the observed RS behavior. Highly stable QC for R_{LRS} was observed and shown to be highly controllable by varying the compliance current. In this manner, R_{LRS} can be precisely modulated over 1 order of magnitude, which is indicative of the potential of single-crystal anatase TiO_2 RRAM devices for scaling to atomic dimensions, and their potential suitability for implementation of approaches for increasing memory storage density using multilevel cells. We postulate that the single-crystal nature of the film plays a key role in suppressing the background current, and therefore in the emergence of QC, and provide evidence that different values of QC are attained via control over the atomic-scale dimensions of single conducting filaments. These results suggest that single-crystal anatase TiO_2 films epitaxially grown on Si are particularly intriguing and promising as a platform for memory based on RS and suggest a variety of directions for future explorations of performance, reliability, and scaling potential of these devices.

■ ASSOCIATED CONTENT

Supporting Information

XPS characterization of the epitaxial single-crystal TiO_2 films. This material is available free of charge via the Internet at http://pubs.acs.org.

■ AUTHOR INFORMATION

Corresponding Author

*E-mail: ety@ece.utexas.edu.

Notes

The authors declare no competing financial interest.

■ ACKNOWLEDGMENTS

The authors would like to thank Stefano Larentis and Leonard F. Register for helpful discussions. This work is partially supported by the National Science Foundation (Award DMR-1006725 and DMR-1207342), Office of Naval Research (Grant N00014-10-10489) and the Judson S. Swearingen Regents Chair in Engineering at The University of Texas at Austin.

■ REFERENCES

(1) Pavan, P.; Bez, R.; Olivo, P.; Zanoni, E. *Proc. IEEE* **1997**, *85*, 1248−1271.

(2) Waser, R.; Aono, M. *Nat. Mater.* **2007**, *6*, 833−840.

(3) Waser, R.; Dittmann, R.; Staikov, G.; Szot, K. *Adv. Mater.* **2009**, *21*, 2632−2663.

(4) Wong, H.-S. P.; Lee, H.-Y.; Yu, S.; Chen, Y.-S.; Wu, Y.; Chen, P.-S.; Lee, B.; Chen, F. T.; Tsai, M.-J. *Proc. IEEE* **2012**, *100*, 1951−1970.

(5) Kim, S. K.; Kim, K. M.; Jeong, D. S.; Jeon, W.; Yoon, K. J.; Hwang, C. S. *J. Mater. Res.* **2013**, *28*, 313−325.

(6) Choi, B. J.; Jeong, D. S.; Kim, S. K.; Rohde, C.; Choi, S.; Oh, J. H.; Kim, H. J.; Hwang, C. S.; Szot, K.; Waser, R.; Reichenberg, B.; Tiedke, S. *J. Appl. Phys.* **2005**, *98*, 033715.

(7) Jeong, D. S.; Schroeder, H.; Breuer, U.; Waser, R. *J. Appl. Phys.* **2008**, *104*, 123716.

(8) Yang, J. J.; Pickett, M. D.; Li, X.; Ohlberg, D. A. A.; Stewart, D. R.; Williams, R. S. *Nat. Nanotechnol.* **2008**, *3*, 429−433.

(9) Strukov, D. B.; Snider, G. S.; Stewart, D. R.; Williams, R. S. *Nature* **2008**, *453*, 80−83.

(10) Pershin, Y. V.; Di Ventra, M. *IEEE Trans. Circuits Syst.* **2010**, *57*, 1857−1864.

(11) Borghetti, J.; Snider, G. S.; Kuekes, P. J.; Yang, J. J.; Stewart, D. R.; Williams, R. S. *Nature* **2010**, *464*, 873−876.

(12) Kim, K. M.; Jeong, D. S.; Hwang, C. S. *Nanotechnology* **2011**, *22*, 254002.

(13) Kim, K. M.; Choi, B. J.; Shin, Y. C.; Choi, S.; Hwang, C. S. *Appl. Phys. Lett.* **2007**, *91*, 012907.

(14) Kim, K. M.; Choi, B. J.; Lee, M. H.; Kim, G. H.; Song, S. J.; Seok, J. Y.; Yoon, J. H.; Han, S.; Hwang, C. S. *Nanotechnology* **2011**, *22*, 254010.

(15) Jeong, D. S.; Schroeder, H.; Waser, R. *Electrochem. Solid-State Lett.* **2007**, *10*, G51−G53.

(16) Park, S.-J.; Lee, J.-P.; Jang, J. S.; Rhu, H.; Yu, H.; You, B. Y.; Kim, C. S.; Kim, K. J.; Cho, Y. J.; Baik, S.; Lee, W. *Nanotechnology* **2013**, *24*, 295202.

(17) Kim, K. M.; Kim, G. H.; Song, S. J.; Seok, J. Y.; Lee, M. H.; Yoon, J. H.; Hwang, C. S. *Nanotechnology* **2010**, *21*, 305203.

(18) Kim, S.; Jeong, H. Y.; Kim, S. K.; Choi, S.-Y.; Lee, K. J. *Nano Lett.* **2011**, *11*, 5438−5442.

(19) Song, S. J.; Seok, J. Y.; Yoon, J. H.; Kim, K. M.; Kim, G. H.; Lee, M. H.; Hwang, C. S. *Sci. Rep.* **2013**, *3*, 3443.

(20) Park, S.-G.; Magyari-Köpe, B.; Nishi, Y. *IEEE Electron Device Lett.* **2011**, *32*, 197−199.

(21) Kamiya, K.; Yang, M. Y.; Park, S.-G.; Magyari-Köpe, B.; Nishi, Y.; Niwa, M.; Shiraishi, K. *Appl. Phys. Lett.* **2012**, *100*, 073502.

(22) Kwon, D.-H.; Kim, K. M.; Jang, J. H.; Jeon, J. M.; Lee, M. H.; Kim, G. H.; Li, X.-S.; Park, G.-S.; Lee, B.; Han, S.; Kim, M.; Hwang, C. S. *Nat. Nanotechnol.* **2010**, *5*, 148−153.

(23) Strachan, J. P.; Pickett, M. D.; Yang, J. J.; Aloni, S.; Kilcoyne, A. L. D.; Medeiros-Ribeiro, G.; Williams, R. S. *Adv. Mater.* **2010**, *22*, 3573−3577.

(24) Hu, C.; McDaniel, M. D.; Ekerdt, J. G.; Yu, E. T. *IEEE Electron Device Lett.* **2013**, *34*, 1385−1387.

(25) Datta, S. *Electronic Transport in Mesoscopic Systems*; Cambridge University Press: New York, 1997.

(26) Terabe, K.; Hasegawa, T.; Nakayama, T.; Aono, M. *Nature* **2005**, *433*, 47−50.

(27) Tappertzhofen, S.; Valov, I.; Waser, R. *Nanotechnology* **2012**, *23*, 145703.

(28) Hasegawa, T.; Terabe, K.; Tsuruoka, T.; Aono, M. *Adv. Mater.* **2012**, *24*, 252−267.

(29) Zhu, X.; Su, W.; Liu, Y.; Hu, B.; Pan, L.; Lu, W.; Zhang, J.; Li, R.-W. *Adv. Mater.* **2012**, *24*, 3941−3946.

(30) Chen, C.; Gao, S.; Zeng, F.; Wang, G. Y.; Li, S. Z.; Song, C.; Pan, F. *Appl. Phys. Lett.* **2013**, *103*, 043510.

(31) Mehonic, A.; Vrajitoarea, A.; Cueff, S.; Hudziak, S.; Howe, H.; Labbé, C.; Rizk, R.; Pepper, M.; Kenyon, A. J. *Sci. Rep.* **2013**, *3*, 2708.

(32) Long, S.; Lian, X.; Cagli, C.; Cartoixà, X.; Rurali, R.; Miranda, E.; Jiménez, D.; Perniola, L.; Liu, M.; Suñé, J. *Appl. Phys. Lett.* **2013**, *102*, 183505.

(33) Miranda, E.; Mehonic, A.; Suñé, J.; Kenyon, A. J. *Appl. Phys. Lett.* **2013**, *103*, 222904.

(34) Long, S.; Perniola, L.; Cagli, C.; Buckley, J.; Lian, X.; Miranda, E.; Pan, F.; Liu, M.; Suñé, J. *Sci. Rep.* **2013**, *3*, 2929.

(35) McDaniel, M. D.; Posadas, A.; Ngo, T. Q.; Dhamdhere, A.; Smith, D. J.; Demkov, A. A.; Ekerdt, J. G. *J. Vac. Sci. Technol., B* **2012**, *30*, 04E111.

(36) McDaniel, M. D.; Posadas, A.; Wang, T.; Demkov, A. A.; Ekerdt, J. G. *Thin Solid Films* **2012**, *520*, 6525−6530.

(37) Mayer, J. T.; Diebold, U.; Madey, T. E.; Garfunkel, E. *J. Electron Spectrosc. Relat. Phenom.* **1995**, *73*, 1−11.

(38) Agrawal, A.; Lin, J.; Zheng, B.; Sharma, S.; Chopra, S.; Wang, K.; Gelatos, A.; Mohney, S.; Datta, S. *VLSI Technol.* **2013**, T200−T201.
(39) Ielmini, D.; Nardi, F.; Cagli, C. *IEEE Trans. Electron Devices* **2011**, *58*, 3246−3253.
(40) Ielmini, D. *IEEE Trans. Electron Devices* **2011**, *58*, 4309−4317.
(41) Ielmini, D. *Tech. Dig. - Int. Electron Devices Meet.* **2011**, 409−412.
(42) Valov, I.; Waser, R.; Jameson, J. R.; Kozicki, M. N. *Nanotechnology* **2011**, *22*, 254003.
(43) Wong, H.-S. P.; Raoux, S.; Kim, S. B.; Liang, J.; Reifenberg, J. P.; Rajendran, B.; Asheghi, M.; Goodson, K. E. *Proc. IEEE* **2010**, *98*, 2201−2227.
(44) Ciancio, R.; Carlino, E.; Rossi, G.; Aruta, C.; Scotti di Uccio, U.; Vittadini, A.; Selloni, A. *Phys. Rev. B* **2012**, *86*, 104110.
(45) Valov, I.; Linn, E.; Tappertzhofen, S.; Schmelzer, S.; van den Hurk, J.; Lentz, F.; Waser, R. *Nat. Commun.* **2013**, *4*, 1771.
(46) Ohno, T.; Hasegawa, T.; Tsuruoka, T.; Terabe, K.; Gimzewski, J. K.; Aono, M. *Nat. Mater.* **2011**, *10*, 591−595.
(47) Valov, I.; Sapezanskaia, I.; Nayak, A.; Tsuruoka, T.; Bredow, T.; Hasegawa, T.; Staikov, G.; Aono, M.; Waser, R. *Nat. Mater.* **2012**, *11*, 530−535.